Artigo

ONE-POT SYNTHESIS OF A REVERSIBLE AND SENSITIVE FLUORESCENT PROBE FOR THE DETECTION OF MALACHITE GREEN

Jinfeng Zhou[a,*] and Chunjie Chu[b]
[a]College of Chemistry and Environmental Engineering, Pingdingshan University, Pingdingshan 467000, China
[b]College of Resources and Environmental Science, Pingdingshan University, Pingdingshan 467000, China

Recebido em 04/04/2022; aceito em 10/08/2022; publicado na web em 13/09/2022

In this work, a recyclable and sensitive fluorescent nanoprobe, RhoB@ZIF-8 composite, has been designed and successfully synthesized by encapsulating rhodamine B (abbreviated as RhoB) into the cavities of zeolitic imidazolate framework-8 (ZIF-8) metal-organic frameworks (MOFs) through a facile one-pot method under mild conditions. The RhoB@ZIF-8 composite exhibited an emission band at 589 nm with fluorescent quantum yield of 19.8%. Since there was an efficient overlap between the absorption of malachite green (MG) and the fluorescence spectra (excitation and emission bands) of RhoB@ZIF-8 composite, the fluorescence intensity decreased sharply after MG was added. The fluorescence quenching was linear with the concentration of MG in the range of 0 to 13.0 μM with a low limit of detection (LOD) of 0.089 μM. Remarkably, this proposed sensing system has good performances including high specificity, good stability and recyclability. Finally, this fluorescent probe was successfully applied to the detection of MG in aquaculture water and fish tissue samples, revealing its potential practicability. This work will provide us a new research platform for MG sensing.

Keywords: MOFs material; ZIF-8; fluorescent detection; malachite green; rhodamine B.

INTRODUCTION

Malachite green (MG for short), as a triarylmethane dye, has been widely used as a cheap and powerful antifungal reagent in aquaculture.[1,2] However, it has been reported that MG is highly toxic, persistent and carcinogenic.[3] The large-scale use of MG exacerbates the pollution of the ecosystem and threatens public health and food safety.[4,5] Thus, the application of MG in aquaculture has been explicitly forbidden in many countries.[6,7] However, MG is still illegally abused due to its low cost. Therefore, the rapid and selective detection of MG has become one of the urgent issues. To date, the detection methods of MG mainly include high performance liquid chromatography (HPLC),[8] surface-enhanced Raman spectroscopy (SERS),[9-11] spectrophotometry.[12-15] HPLC techniques require complex pre-treatment and expensive equipment, and can only be operated in the laboratory.[5] For SERS methods, substrate unreliability and impurity interference seriously inhibit their practical applications.[16] Among them, fluorescence-based methods have found wide applications in various fields due to their fast response, signal visualization, high sensitivity and simple operation.[13-15] In addition, fluorescence methods exhibit unique advantages, especially their eye-readable capability for analyte detection with the help of a ultraviolet (UV) lamp, and this technology has now developed into one of the most popular analysis methods.[15] Thus, it is highly desirable to develop a sensitive and reversible fluorescent sensor for the detection of MG.

Metal-organic frameworks (MOFs), as a new type of crystalline porous materials, have received increased attention across a number of disciplines in recent years due to their high porosity, large surface area and tunable framework structure.[17-20] Thus far, a large number of literatures have reported that MOFs were used as carriers to stabilize and disperse guest molecules to prepare host-guest composites, and then used them in detecting metal ions, biological small molecules, organic volatile solvents, etc.[21-24] More importantly, compared with other fluorescent probes, MOFs can selectively absorb and enrich analytes to amplify sensing signals.[25] As a typical representative of MOFs, zeolitic imidazolate framework-8 (ZIF-8), characterized by sodalite zeolite-type structural and featuring large cavities (11.6 Å) and small apertures (3.4 Å), has been widely utilized in a wide of different fields because of their chemical robustness and thermal stability, ease of synthesis and the ability as a host matrix.[25-30] Based on the above advantages, ZIF-8 can be deemed to be an ideal host candidate for trapping the guest molecules to prepare ZIF-based composite for different purposes.

Up to now, only a few MG fluorescent probes based on MOFs composites have been reported.[31-34] For example, Zhang and co-workers designed a Eu (III)-functionalized nanoscale MOF probe Eu^{3+}@MIL-53(Al) by encapsulating Eu^{3+} in MIL-53 (Al), which functioned as "turn-off" sensor through fluorescence resonance energy transfer for the MG detection.[31] Zheng and his coworkers synthesized a europium-based MOFs (Eu-TDA) and investigated its applications in luminescent sensing of MG.[32] Du *et al.* fabricated a Tb-based MOFs fluorescent probe and then utilized it in detecting MG.[33] A Eu^{3+} functionalized Zr-MOF-808 probe by post-synthetic modification for the monitoring MG has been reported by Zhang and co-workers.[34] From these fluorescent probes, they are all based on rare earth metal Eu or Tb functionalized MOFs. The fluorescent dye@MOFs composites for the determination of MG have never been reported. Therefore, it is of great significance to prepare dye@MOFs composites by a simple method for the sensing MG.

In this work, a simple and sensitive fluorescent probe RhoB@ZIF-8 composite for the detection of MG has been designed and fabricated by encapsulating RhoB into ZIF-8 cavities through a facile one-pot synthesis. Since there is an efficient spectra overlay between the absorption of MG and the excitation and emission spectra of RhoB@ZIF-8 composite, the fluorescence of RhoB@ZIF-8 composite can be effectively quenched by MG. Therefore, a sensitive MG fluorescence sensor was established. This RhoB@ZIF-8 nanoprobe shows good sensitivity, selectivity, reversibility and recyclability in detecting trace amount of MG.

*e-mail: zhoujf016@163.com

EXPERIMENTAL SECTION

Materials and instruments

All chemicals were purchased from commercial sources and directly used without further purification unless otherwise noted. UV-Vis absorption spectra were obtained on a Perkin Elmer Lambda 35 spectrophotometer. Powder X-ray diffraction (PXRD) data were recorded on a Bruker D8 Advance diffractometer equipped with Cu K_α radiation (λ = 1.5406 Å). The gas sorption experiments were measured on a Micromeritics 3Flex automated micropore gas analyzer. Scanning electron microscopy (SEM) images were recorded on a SU8010 field-emission scanning electron microscope. Transmission electron microscopy (TEM) images were performed on a transmission electron microscope (FEI Tecnai G2 F20). The particle sizes were determined using a dynamic light scattering analyzer (Malvern, Zetasizer Nano). The fluorescence spectra were carried out by a F-7000 spectrophotometer. The fluorescent quantum yields were measured using a QY-2000 spectrophotometer equipped with an $BaSO_4$-coating integrated sphere (Orient KOJI, China). Nanosecond lifetimes were measured on a FluoroLog-3-TCSPC (Horiba Scientific, Edison) using a TCSPC MCA model equipped with a picosecond photodetector (<200 ps) (PPD850) and a picosecond laser (duration is 180 ps, Deltadiode, 100 MHz laser). DeltaDiode-370 picosecond pulsed laser was used for nanosecond lifetime measurements.

Synthesis of RhoB@ZIF-8 composite

The synthesis route of RhoB@ZIF-8 composite is different from that reported in literatures.[35,36] In a typical synthesis, 0.5 mL RhoB aqueous solution (0.01 mol L^{-1}) and 10.0 g 2-methylimidazole aqueous solution containing 2.0 g 2-methylimidazole and 8.0 g H_2O were mixed. Subsequently, 0.2 g $Zn(NO_3)\cdot 6H_2O$ dissolved 1.0 mL H_2O was added into the above reaction solution, and then this mixture was vigorously stirred for 15 min at room temperature. After the reaction, the RhoB@ZIF-8 composite was collected by centrifugation and washed several times with water and ethanol until the supernatant became colorless. Finally, the powder product was dried at room temperature under vacuum.

For comparison, the pure ZIF-8 was prepared in a similar way without adding RhoB molecules.

The loading amount of RhoB in RhoB@ZIF-8 composite

ZIF-8 decomposes under strong acid conditions, so RhoB molecules can be released. Firstly, the linear relationship between concentrations of RhoB and absorbance at 553 nm was established. Subsequently, the RhoB@ZIF-8 composite was dissolved in a nitric acid solution (0.1 mol L^{-1}) and determined by UV-vis spectroscopy. Finally, the loading amount of RhoB in RhoB@ZIF-8 composite was determined according to absorbance at 553 nm and the regression equation of linear curve (Figure 1S).

Sample preparation for the particle size distribution

3.0 mg ZIF-8 or RhoB@ZIF-8 composite was respectively dispersed in 3.0 mL H_2O, and the suspension was mixed thoroughly under ultrasonication. The particle sizes were measured by a dynamic light scattering. Each sample was determined three times, and the particle size distribution was obtained by taking the average value.

Sample preparation for photophysical studies

In the fluorescence response experiment setup, 6.0 mg RhoB@ZIF-8 composite was added into 3.0 mL distilled water and dispersed uniformly through ultrasound. This suspension was transferred to 1 cm quartz cuvette, and the fluorescence spectra were measured in-situ after different amounts of MG were added. Throughout the fluorescence test, the excitation wavelength was set as 540 nm. The excitation and emission slit widths were all 5 nm.

Detection of MG in real samples

MG in aquaculture water and fish tissue was detected by standard addition method. Aquaculture water samples were collected from a local fish pond. Fishes were brought from a local supermarket. For aquaculture water samples, they were filtered firstly by 0.22 μM filter membrane. Subsequently, MG with different concentrations (3.0, 6.0 and 9.0 μM) were added into the actual samples for fluorescence detection. For fish samples, they were pretreated in reference to the method reported in the literature with some modification.[37,38] Firstly, 10 g of back muscle was crushed in a grinder and put into a beaker. Then, 30 mL of CH_3CN and 120 mL phosphate buffer containing different concentrations of MG (3.0, 6.0 and 9.0 μM) were added into the above beaker. Next, the mixture was ultrasonicated for 1 hour and the supernatant was collected by centrifugation. Finally, 6 mg RhoB@ZIF-8 composite was mixed with the 3.0 mL of the as-prepared aquaculture water and fish tissue samples for fluorescence measurement.

RESULTS AND DISCUSSION

Preparation and structural characterization of RhoB@ZIF-8 composite

RhoB was used as the guest molecules because of the fascinating emission property and suitable size.[25,39] ZIF-8 was selected as the host material due to the relatively large pore size, outstanding stability and ease of synthesis.[25-30] The RhoB@ZIF-8 composite was synthesized by encapsulating RhoB molecules into the framework of ZIF-8 through a facile one-pot in situ self-assembly approach for which the preparation process is demonstrated in Scheme 1. In short, by mixing RhoB molecules with $Zn(NO_3)\cdot 6H_2O$ and 2-MeIm in water at RT for just fifteen minutes, RhoB@ZIF-8 composite can be successfully formed.

The structural characterization of RhoB@ZIF-8 composite was fully studied by PXRD, SEM, TEM, N_2 absorption-desorption isotherms and absorption spectra. As shown in Figure 1, the peaks for ZIF-8 at 2θ = 7.4°, 10.3°, 12.9°, 14.7°, 16.5° and 18.0° can be attributed to (011), (002), (022), (013), (112) and (222), respectively, which are consistent with the reported ZIF-8 previously.[40,41] The PXRD patterns of RhoB@ZIF-8 composite are identical with those of simulated ZIF-8, clearly indicating that the encapsulation with RhoB molecules has negligible effect on the lattice distortion of ZIF-8. Compared to the strong diffraction peaks of ZIF-8, peaks associated with RhoB molecules within the crystals were too weak to be observed clearly, presumably because of their low concentrations and/or small sizes.[42] The existence of RhoB molecules in the RhoB@ZIF-8 composite can be confirmed by the obvious color change from white of ZIF-8 to magenta of RhoB@ZIF-8 composite under natural light (the inset in Figure 1). Subsequently, the loading amount of RhoB molecules in RhoB@ZIF-8 composite was calculated to be 5.8 wt% by measuring the UV-vis absorption spectra after the composite was decomposed in a nitric acid solution. The SEM and TME images

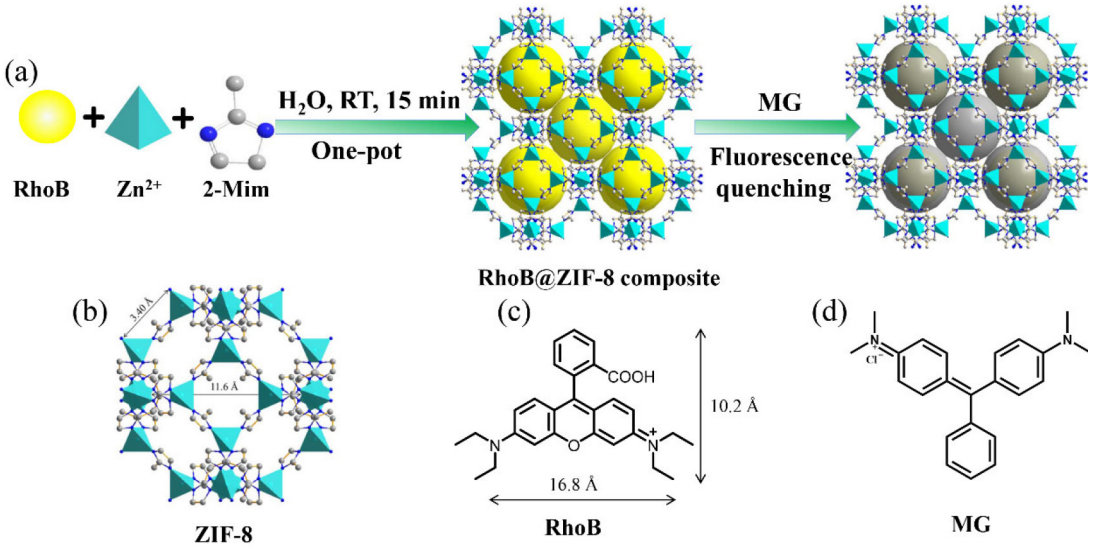

Scheme 1. *Illustration of the fabrication process of the RhoB@ZIF-8 composite and its application in sensing MG*

display that RhoB@ZIF-8 composite and ZIF-8 display near rhombic dodecahedron shape (Figure 2). As displayed in Figure 2S, the particle sizes of ZIF-8 and RhoB@ZIF-8 composite were calculated as ~460 nm and ~390 nm, respectively. The porosity and surface-area changes before and after the encapsulation of RhoB molecules were examined by N_2 absorption-desorption isotherms at 77 K. It can be seen from Figure 3a that the absorption-desorption processes have the characteristics of typical Type-I isothermal absorption according to IUPAC classification method. The Brunauer-Emmett-Teller (BET) surface areas of ZIF-8 and RhoB@ZIF-8 composite were measured to be 1938 and 1721 m^2/g, respectively, which clearly manifests that the guest molecules were successfully encapsulated in the ZIF-8 scaffold and occupied some of the space. Moreover, the pore-size distribution simulated by the Barrett-Joyner-Halenda (BJH) adsorption method suggests that incorporation of RhoB molecules does not alter the pore size of ZIF-8, which is consistent with those reported previously (inset in Figure 3b).[42,43] However, the value of dv/dW dramatically decreases from ZIF-8 to RhoB@ZIF-8 composite. This difference in the dv/dW data indirectly confirmed the inclusion of RhoB molecules into ZIF-8 due to the influence on the micropores distribution.[44] In order to further confirm that RhoB molecules were successfully captured into the ZIF-8 channels, UV-vis absorption spectra of the ZIF-8, free RhoB and RhoB@ZIF-8 composite were carried out (Figure 3b). A specific absorption peak at 554 nm for RhoB@ZIF-8 composite is observed, which is consistent with that of free RhoB. These results suggest that RhoB molecules are well loaded into the frameworks of ZIF-8.

In order to further clarify whether the RhoB molecules were adsorbed on the outer surface or encapsulated inside the ZIF-8 cavities, a series experiments were carried out. The zeta potential of ZIF-8 was first measured to be 21.2 mV. Thus, ZIF-8 is positively charged. It is well-known that RhoB molecule is a cationic dye.[35,45] Therefore, RhoB molecules are difficult to be adsorbed on the surface of ZIF-8. To further verify this conclusion, the mixture of ZIF-8 and RhoB was prepared as follows: First 0.5 mL RhoB aqueous solution (0.01 mol L^{-1}) and ZIF-8 (100 mg) in water (10 mL) were mixed with stirring at room temperature. After 5 hours, the suspension was collected by centrifugation and washed successively with H_2O and ethanol, respectively. Finally, a white powder product was obtained, indicating that RhoB molecules were not absorbed on the surface of ZIF-8. Additionally, RhoB@ZIF-8 composite was immersed

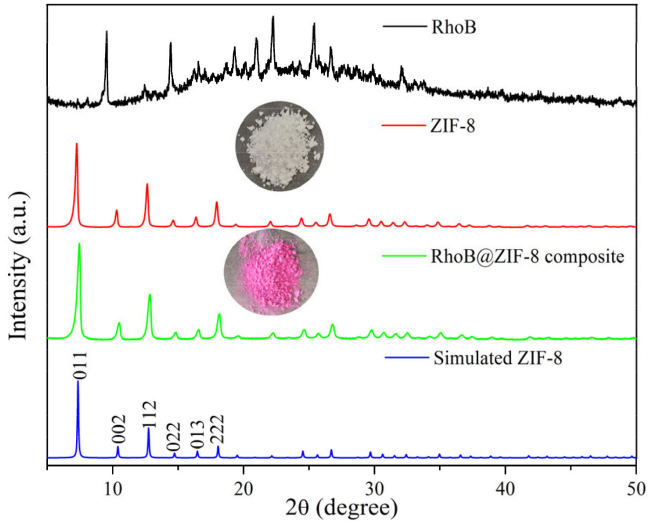

Figure 1. *PXRD patterns of RhoB@ZIF-8 composite, as-synthesized ZIF-8, simulated ZIF-8 and RhoB. The photographs of RhoB@ZIF-8 composite and as-synthesized ZIF-8 under natural light are shown in the inset*

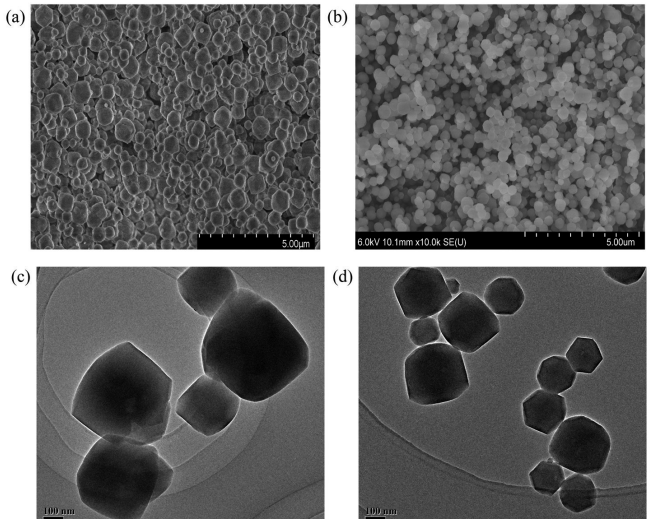

Figure 2. *(a) The SEM images of ZIF-8. (b) The SEM image of RhoB@ZIF-8 composite. (c) The TEM image of ZIF-8. (d) The TEM image of RhoB@ZIF-8 composite*

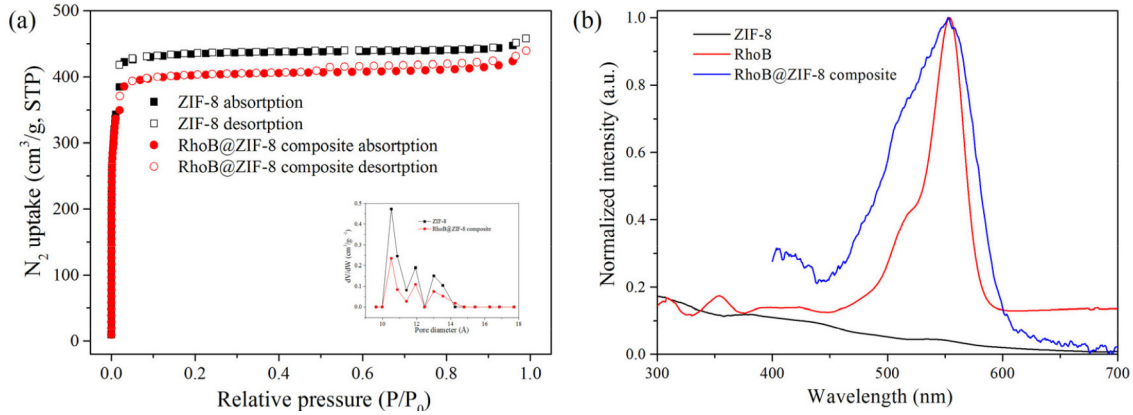

Figure 3. *(a) N_2 adsorption-desorption isotherms for ZIF-8 and RhoB@ZIF-8 composite at 77 K. Inset: The pore size distribution for ZIF-8 and RhoB@ZIF-8 composite using data measured with N_2 at 77 K. (b) The absorption spectra of RhoB aqueous solution, ZIF-8 and RhoB@ZIF-8 powder*

in ethanol, and the supernatant was colorless and had no visible fluorescence, demonstrating that RhoB molecules were firmly fixed in the frameworks of ZIF-8. All in all, the above results richly manifest that RhoB molecules were trapped in the ZIF-8 cavity.

Fluorescent properties of RhoB@ZIF-8 composite

The photoluminescence properties of RhoB@ZIF-8 composite were comprehensively studied by fluorescence emission spectra. Firstly, three-dimensional excitation-emission matrix (3D-EEM) fluorescence spectra of RhoB aqueous solution, ZIF-8 and RhoB@ZIF-8 powder were measured, respectively (Figure 4a, Figure 3S and 4S). RhoB aqueous solution showed a strong emission band at 585 nm. However, due to the aggregation quenching effect, its solid-state has weak fluorescence. For RhoB@ZIF-8 composite, an evident emission band located at 589 nm is observed (Figure 4 and Figure 5Sd). Under 365 nm UV light, RhoB@ZIF-8 suspension emits bright yellow light (the inset in Figure 4b). The fluorescent quantum yield was measured to be 19.8%. By comparing the 3D-EEM spectra of RhoB@ZIF-8 composite with these of ZIF-8 powder and RhoB aqueous solution, it can be clearly concluded that the emission band at 589 nm of RhoB@ZIF-8 composite origins from RhoB molecules. This further indicates that RhoB molecules were loaded into the ZIF-8 frameworks. Thanks to the shell-isolation of ZIF-8 MOFs, the aggregation and collision of RhoB fluorescent molecules were reduced, thus effectively inhibiting the aggregation quenching effect and significantly improving the emission property of RhoB coated into ZIF-8 cavities.

Good photostability is crucial precondition for the practical applications. In order to investigate the photostability, the fluorescence spectrum of RhoB@ZIF-8 suspension was recorded every day (Figure 6S), the luminescence was basically unaffected within five days. Therefore, it is obvious that RhoB@ZIF-8 suspension exhibits outstanding photostability.

Fluorescent properties of RhoB@ZIF-8 composite

The detection of MG was conducted by recording the fluorescence spectra change of the suspension of RhoB@ZIF-8 composite under various concentrations of MG (Figure 5). As illustrated in Figure 5a, with increasing content of MG, the emission band of 589 nm significantly quenched. Only 32.0 μM MG was added, the fluorescence intensity was quenched by 90%. The detection sensitivity of RhoB@ZIF-8 composite toward MG can be rationally quantified by adopting the Stern-Volmer (SV) equation ($F_0/F = K_{sv}$ [MG] + 1, where F_0 and F are the fluorescence intensity in the absence and presence of MG, respectively. [MG] is the molar concentration of MG and K_{sv} is the quenching constant). Figure 5b shows the linear relationship between F_0/F and the concentrations of MG in the range of 0 to 13.0 μM, a good linear correlation (R^2 = 0.9969) can be obtained. The K_{sv} value was determined as 2.27 × 10^5 M^{-1} according to the linear regression equation. Meanwhile, the detection limit (LOD) was calculated to be 0.089 μM (LOD = 3σ/k, σ is the standard deviation of 11 blank measurements and k is the slope of linear regression equation), implying the high sensing sensitivity of RhB@ZIF-8 nanoprobe toward MG. A comparison of this method with other

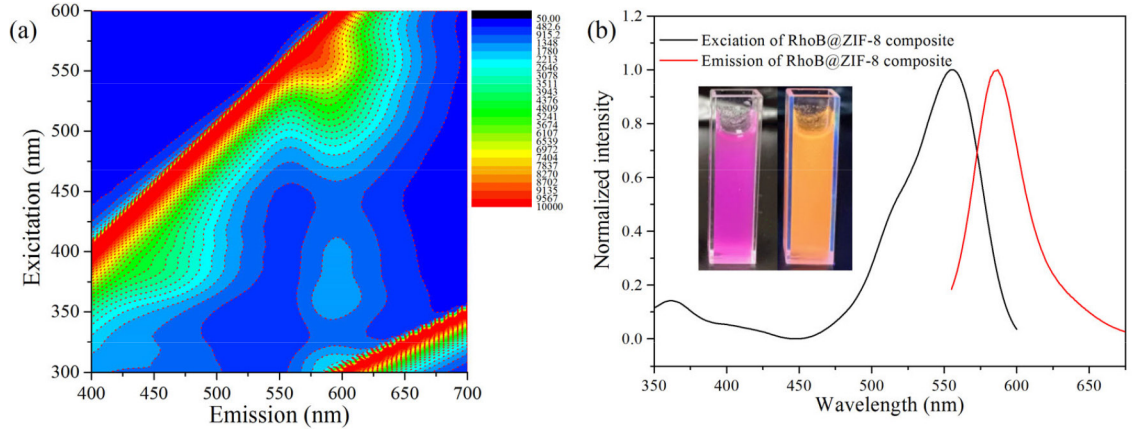

Figure 4. *(a) 3D-EEM spectrum of RhoB@ZIF-8 powder. (b) The excitation and emission spectra of RhoB@ZIF-8 powder. Inset: the photograph of RhoB@ZIF-8 composite under natural light (left) and 365 nm UV light (right)*

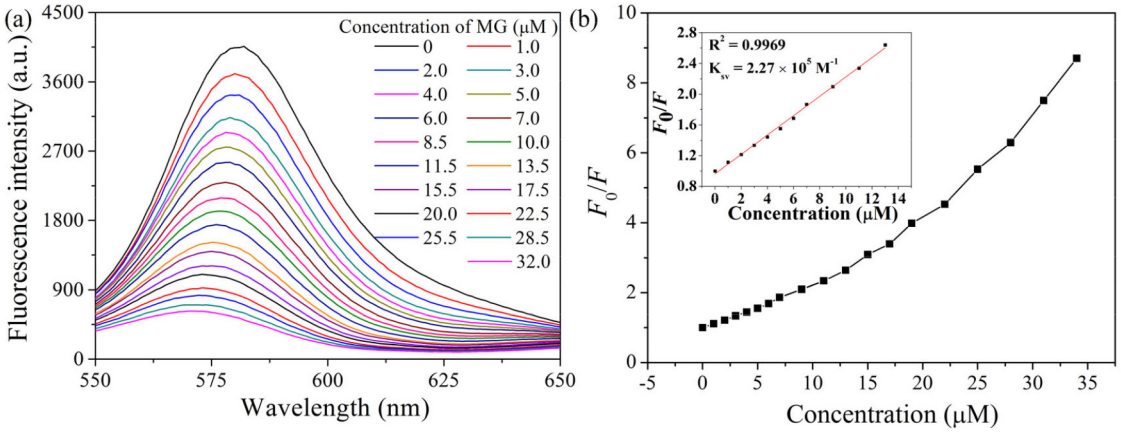

Figure 5. *(a) Fluorescence emission spectra of RhoB@ZIF-8 composite as a function of MG concentration. (b) Relationship between F_0/F at 589 nm and the concentration of MG in the range of 0-32.0 μM. Inset shows the linear relationship between F_0/F at 589 nm and MG concentration in the range of 0-13.0 μM*

nanomaterial-related fluorescence methods for MG detection is shown in Table 1S. It can be seen that the detection range and LOD of this proposed method are comparable to those of some reported methods.

In order to better illustrate the specificity of RhB@ZIF-8 composite toward MG, the fluorescence responses in the presence of some potential coexisting interferents including common metal ions, anions and several physiological substances were examined. As illustrated in Figure 6a and Figure 7S, only MG can cause significant fluorescence intensity quenching, while interferents even at high concentration (10 equiv.) show a negligible effect, which further confirms the RhoB@ZIF-8 composite is a highly selective probe for MG sensing in complex matrix.

Recyclability is a key parameter to evaluate the practicability of a sensor. The recycling performance of the RhoB@ZIF-8 composite as a fluorescent probe toward MG was studied in detail (Figure 6b). When MG was added into the aqueous suspension of the RhoB@ZIF-8 probe, the emission band at 589 nm quenched significantly. After MG was detected, the suspension of the probe was collected by centrifugation and washed with water several times. The redispersed suspension could recover to almost the same F_{589} value with that of the original sample after five consecutive cycles. Meanwhile, the SEM image (Figure 8S) after fifth cycles sensing of MG suggest that this probe still maintained its pristine structure. Therefore, these results reveal that the RhoB@ZIF-8 fluorescent probe is easily recyclable and completely reversible, which offers a facile and economical method for practical application.

Sensing mechanism

In order to further gain insight into the fluorescence quenching mechanism, a series of test experiments were conducted. Firstly, the absorption spectrum of MG and the fluorescence spectra of RhoB@ZIF-8 composite were compared. As illustrated in Figure 7a, MG aqueous solution exhibits a broad absorption from 300 and 700 nm, covering the excitation and emission bands of RhoB@ZIF-8 composite. Inner filter effect (IFE) can take place if the absorption spectrum of a quencher greatly overlaps with the excitation and/or emission of a fluorophore. In addition, the absorption spectrum of MG covers the emission band of RhoB@ZIF-8 composite, it is possible to transfer energy from RhoB@ZIF-8 composite to MG through fluorescence resonance energy transfer (FRET). Thus, the fluorescence quenching phenomenon of RhoB@ZIF-8 composite by MG is probably caused by IFE or FRET. The fluorescence decay lifetime of a fluorescent probe remains unchanged in IFE but obvious shortens in FRET. To further verify the quenching mechanism, the fluorescence lifetimes of the suspension of RhoB@ZIF-8 composite in the absence and presence of MG were measured. As displayed in Figure 7b, the lifetimes of RhoB@ZIF-8 composite show a negligible change after adding 10.0 μM MG, indicating that MG-induced fluorescence quenching of RhoB@ZIF-8 was mainly due to IFE.

Detection of MG in real samples

To verify the practicability of this proposed method, MG in aquaculture water and fish tissue were detected by standard addition method. As listed in Table 1, the recoveries of MG are between 98.2% and 106.3% with the relative standard deviation in the range

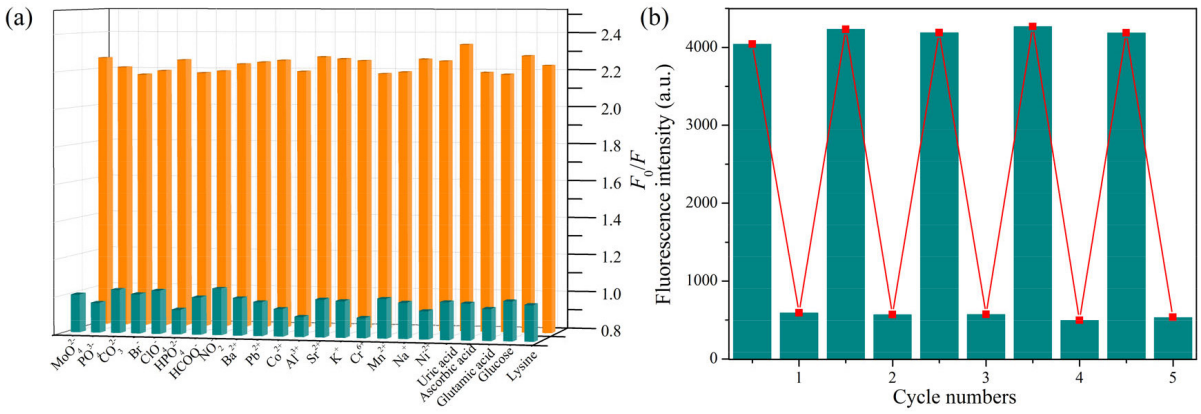

Figure 6. *(a) Fluorescence response of RhoB@ZIF-8 composite toward MG (10 μM) in the presence of other potential coexisting interferents (100 μM). (b) Recyclability of RhoB@ZIF-8 composite for the detection of MG*

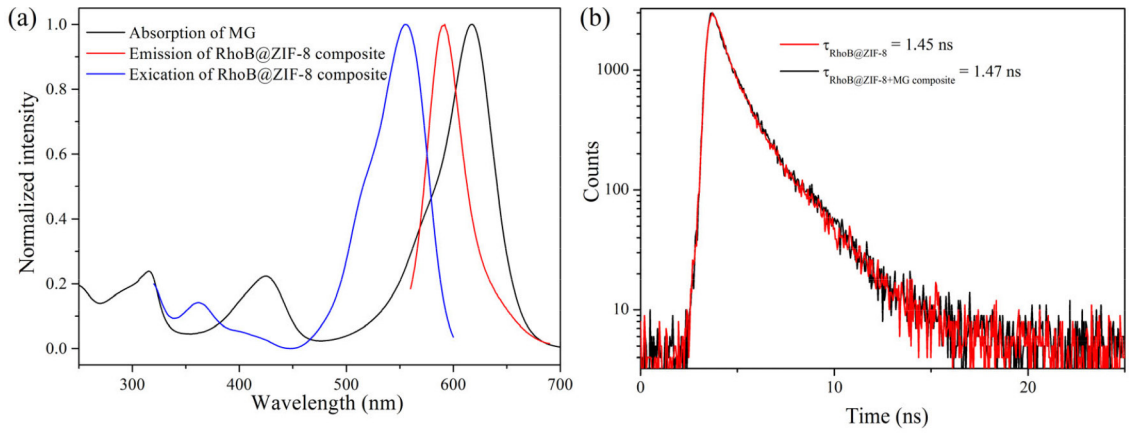

Figure 7. *(a) The absorption spectrum of MG and fluorescence excitation and emission spectra of RhoB@ZIF-8 composite. (b) Fluorescence decay plots of the suspension of RhoB@ZIF-8 composite in the absence and presence of 10.0 μM MG*

Table 1. Detection of MG in real samples (n = 3)

Samples	Spiked (μM)	Found (μM)	Recoveries (%)	RSD (%)
Aquaculture water	3.0	3.08	102.7	3.8
	6.0	5.89	98.2	4.5
	9.0	9.38	104.2	2.4
Fish tissue	3.0	2.90	96.7	2.9
	6.0	5.87	97.8	3.4
	9.0	9.57	106.3	2.7

of 2.4-4.5%, indicating that our method is reliable for detection of MG in the real samples.

CONCLUSIONS

In summary, a recyclable and sensitive fluorescent nanoprobe, RhoB@ZIF-8 composite, was successfully fabricated through one-pot in situ self-assembly of 2-methylimidazole, Zn^{2+} and RhoB molecules in water at room temperature. The fluorescence intensity of RhoB@ZIF-8 suspension can be effectively quenched by MG based on the IFE mechanism. This developed IFE-based probe exhibits high specificity, good stability and recyclability, and has been successfully applied in sensing trace amount of MG in aquaculture water and fish tissue samples. The preparation strategy of this fluorescent probe reported in this work is simple, rapid, mild and environmentally friendly, which will provide a new platform for environmental analysis and food monitoring.

SUPPLEMENTARY MATERIAL

Figures 1S to 8S and Table 1S are available in pdf format, free of charge, at http://quimicanova.sbq.org.br.

ACKNOWLEDGEMENTS

This work was funded by the High-Level Talent Research Start-Up Fund, Pingdingshan University (PXY-BSQD-2017003) and a Basic Research Program of Key Scientific Research Projects in Higher Education Institutions in Henan Province (18B150018).

REFERENCES

1. Khan, M. A.; Otero, M.; Kazi, M.; Alqadami, A. A.; Wabaidur, S. M.; Siddiqui, M. R.; Alothman, Z. A.; Sumbul, S.; *J. Hazard. Mater.* **2019**, *365*, 759. [Crossref]
2. Renita, A. A.; Vardhan, K. H.; Kumar, P. S.; Ngueagni, P. T.; Abilarasu, A.; Nath, S.; Kumari, P.; Saravanan, R.; *Chemosphere* **2021**, *273*, 129634. [Crossref]
3. Srivastava, S.; Sinha, R.; Roy, D.; *Aquat. Toxicol.* **2004**, *66*, 319. [Crossref]
4. Wu, J.; Jing, X.; Liu, Y.; Zhao, L.; Ji, X., Fu, H.; Zhang, B.; Zhang, Y.; Wang, S; *Sens. Actuators, B* **2022**, *361*, 2131748. [Crossref]
5. Ma, Z.-B.; Zhang, Y., Ren, X.-H.; He, X.-W.; Li, W.-Y.; Zhang, Y.-K.; *Spectrochim. Acta, Part A* **2022**, *276*, 121196. [Crossref]
6. Lin, Z.-Z.; Zhang, H.-Y.; Peng, A.-H.; Lin, Y.-D.; Li, L.; Huang, Z.-Y.; *Food Chem.* **2016**, *200*, 32. [Crossref]
7. Tian, H.; Li, H.; Fang, Y; *ACS Appl. Mater. Interfaces* **2019**, *11*, 16207. [Crossref]
8. Zhang, L.; Zhang, Y.; Tang, Y.; Li, X.; Zhang, X.; Li, C.; Xu, S. X.; *Int. J. Environ. Anal. Chem.* **2018**, *98*, 215. [Crossref]
9. Deng, D.; Lin, Q.; Li, H.; Huang, Z.; Kuang, Y.; Chen, H.; Kong, J.; *Talanta* **2019**, *200*, 272. [Crossref]
10. Lai, H.; Shang, W.; Yun, Y.; Chen, D.; Wu, L.; Xu, F.; *Microchim. Acta* **2019**, *186*, 144. [Crossref]
11. Zhou, B.; Shen, J.; Li, P.; Ge, M.; Lin, D.; Li, Y. Y.; Lu, J.; Yang, L.; *ACS Appl. Nano Mater.* **2019**, *2*, 2752. [Crossref]
12. Gavrilenko, N. A.; Volgina, T. N.; Pugachev, E. V.; Gavrilenko, M. A.; *Food Chem.*, **2019**, *274*, 242. [Crossref]
13. Luo, X.; Chen, Z.; Li, H.; Li. W.; Cui, L.; Huang, J.; *Analyst* **2019**, *144*, 4204. [Crossref]
14. Ju, Y. J.; Li, N.; Liu, S. G.; Han, L.; Xiao, N.; Luo, H. Q.; Li, N. B.; *Sens. Actuators, B* **2018**, *275*, 244. [Crossref]
15. Yue, X.; Li, Y.; Xu, S.; Li, J.; Li, M.; Jiang, L.; Jie, M.; *Food Chem.* **2022**, *371*, 131164. [Crossref]
16. Chen, D.; Zhu, X.; Huang, J.; Wang, G.; Zhao, Y.; Chen, F.; Wei, J.; Song, Z.; Zhao, Y.; *Anal. Chem.* **2018**, *90*, 9048. [Crossref]
17. Fardjahromi, A. M.; Nazari, H.; Ahmadi Tafti, S. M.; Razmjou, A.; Mukhopadhyay, S.; Warkiani, M. E.; *Mater. Today Chem.* **2022**, *23*, 100670. [Crossref]
18. Karamzadeh, S.; Sanchooli, E.; Oveisi, A. R.; Drliran, S.; Luque, R.; *Appl. Catal. B: Environ.*, **2022**, *303*, 120815. [Crossref]
19. Wang, M. C.; Dong, R. H.; Feng, X. L.; *Chem. Soc. Rev.* **2021**, *50*, 2764. [Crossref]
20. Wang, Y.; Li, J.; Li, X.; Jin, H.; Ali, W.; Song, Z.; Ding, S.; *J. Mater. Chem. A* **2022**, *10*, 699. [Crossref]
21. Wei, Z.; Chen, D.; Guo, Z.; Jia, P.; Xing, H.; *Inorg. Chem.* **2020**, *59*, 5386. [Crossref]
22. Wu, S.; Min, H.; Shi, W.; Cheng, P.; *Adv. Mater.* **2020**, *32*, 1805871. [Crossref]

23. Yang, L.; Liu, Y.-L.; Liu, C.-G.; Ye, F.; Fu, Y.; *J. Hazard. Mater.* **2020**, *381*, 120966. [Crossref]
24. Zhou, X.; Li, J.; Tan, L.-L.; Li, Q.; Shang, L.; *J. Mater. Chem. A* **2020**, *8*, 3661. [Crossref]
25. Ma, Y.; Xu, G.; Wei, F.; Cen, Y.; Xu, X.; Shi, M.; Cheng, X.; Chai, Y.; Sohail, M.; Hu, Q.; *ACS Appl. Mater. Interfaces* **2018**, *10*, 20801. [Crossref]
26. Kumar, A.; Sharma, A.; Chen, Y.; Jones, M. M.; Vanyo, S. T.; Li, C.; Visser, M. B.; Mahajan, S. D.; Sharma, R. K.; Swihart, M. T.; *Adv. Funct. Mater.* **2020**, *31*, 2008054. [Crossref]
27. Liu, Y.; Pang, H.; Wang, X.; Yu, S.; Chen, Z.; Zhang, P.; Chen, L.; Song, G.; Alharbi, N. S.; Rabah, S. O.; Wang, X.; *Chem. Eng. J.* **2021**, *406*, 127139. [Crossref]
28. Please add "Gao, X.; Xue, Y.; Zhu, Z.; Chen, J.; Liu, Y.; Cheng, X.; Zhang, X.; Wang, J.; Pei, X.; Wan, Q.; *ACS Appl. Mater. Interfaces* **2021**, *13*, 97. [Crossref]
29. Park, K. S.; Ni, Z.; Côté, A. P.; Choi, J. Y.; Huang, R.; Uribe-Romo, F. J.; Chae, H. K.; O'Keeffe, M.; Yaghi, O. M.; *Proc. Natl. Acad. Sci. U. S. A.* **2006**, *103*, 10186. [Crossref]
30. Troyano, J.; Carne-Sanchez, A.; Avci, C.; Imaz, I.; Maspoch, D.; *Chem. Soc. Rev*. **2019**, *48*, 5534. [Crossref]
31. Wang, T.; Wang, Y.; Sun, M.; Hanif, A.; Wu, H.; Gu, Q.; Ok, Y. S.; Tsang, D. C. W.; Li, J.; Yu, J.; Shang, J.; *Chem. Sci*. **2020**, *11*, 6670. [Crossref]
32. Yi, K.; Zhang, L.; *Food Chem.* **2021**, *354*, 129584. [Crossref]
33. Han, L.; Kong, Y.-J.; Hou, G.-Z.; Chen, H.-C.; Zhang, X.-M.; Zheng, H.-G.; *Inorg. Chem*. **2020**, *59*, 7181. [Crossref]
34. Wang, X.-T.; Wei, W.; Zhang, K.; Du, S.-W.; *RSC Adv.* **2020**, *10*, 6129. [Crossref]
35. Du, T.; Wang, J.; Zhang, T.; Zhang, L.; Yang, C.; Yue, T.; Sun, J.; Li, T.; Zhou, M.; Wang, J.; *ACS Appl. Mater. Interfaces* **2020**, *12*, 13189. [Crossref]
36. Chaudhari, A. K.; Tan, J.-C.; *Adv. Optical Mater.* **2020**, *8*, 1901912. [Crossref]
37. Zhang, X.-T.; Li, Y.; Zhang, L.; *Spectrochim. Acta Part A Mol. Biomol. Spectrosc.,* **2021**, *251*, 119464. [Crossref]
38. Hu, Y. P.; Gao, Z. J.; Luo, J. F.; *Food Chem*. **2021**, *335*, 127677. [Crossref]
39. Zhang, Y.; Gutiérrez, M.; Chaudhari, A. K.; Tan, J. C.; *ACS Appl. Mater. Interfaces* **2020**, *12*, 37477. [Crossref]
40. Zhang, T.; Zhang, X.; Yan, X.; Kong, L.; Zhang, G.; Liu, H.; Qiu, J.; Yeung, K.; *Chem. Eng. J.* **2013**, *228*, 398. [Crossref]
41. Ebrahim, A. M.; Plonka, A. M.; Rui, N.; Hwang, S.; Gordon, W. O.; Balboa, S. D.; Frenkel, A. I.; *ACS Appl. Mater. Interfaces* **2020**, *12*, 58326. [Crossref]
42. Lu, G.; Li, S.; Guo, Z,; Farha, O. K.; Hauser, B. G.; Qi, X.; Wang, Y.; Wang, X., Han, S.; Liu, X.; DuChene, J. S.; Zhang, H.; Zhang, Q.; Chen, X.; Ma, J.; Loo, S. C. J.; Wei, W. D.; Yang, Y.; Hupp, J. T.; Huo, F.; *Nat. Chem.* **2012**, *4*, 310. [Crossref]
43. Zhao, Z.; Ru, J.; Zhou, P.; Wang, Y.; Shan, C.; Yang, X.; Cao, J.; Liu, W.; Guo, H.; Tang, Y.; *Dalton Trans*. **2019**, *48*, 16952. [Crossref]
44. Zhao, Z.; Ru, J.; Zhou, P.; Wang, Y.; Shan, C.; Yang, X.; Cao, J.; Liu, W.; Guo, H.; Tang, Y.; *Dalton Trans*. **2019**, *48*, 16952. [Crossref]
45. Zhou, J. F.; Zhou, Q.; Chu, C. J.; *Microchem. J.* **2022**, *180*, 107631. [Crossref]